computation

MDPI

Article

Numerical Estimation of the Structural Integrity in an Existing Pipeline Network for the Transportation of Hydrogen Mixture in the Future

Clio Vossou * and Dimitrios Koulocheris

Vehicles Laboratory, School of Mechanical Engineering, National Technical University of Athens, 15772 Zografou, Greece

* Correspondence: klvossou@mail.ntua.gr

Abstract: Hydrogen is gaining attention due to its potential to address key challenges in the sectors of energy, transportation and industry, since it is a much cleaner energy source when compared to fossil fuels. The transportation of hydrogen from the point of its production to the point of use can be performed by road, rail, sea, pipeline networks or a combination of the abovementioned. Being in the preliminary stage of hydrogen use, the utilization of the already existing natural gas pipeline networks for hydrogen mixtures transportation has been suggested as an efficient means of expanding hydrogen infrastructure. Yet, exploring this alternative, major challenges such as the pre-existence of cracks in the pipelines and the effect of hydrogen embrittlement on the material of the pipelines exist. In this paper, the macroscopic numerical modeling of pipeline segments with the use of the finite element method is performed. In more details, the structural integrity of intact and damaged pipeline segments, of different geometry and mechanical properties, was estimated. The effect of the pipeline geometry and material has been investigated in terms of stress contours with and without the influence of hydrogen. The results suggest that the structural integrity of the pipeline segments is more compromised by pre-existing longitudinal cracks, which might lead to an increase in the maximum value of equivalent Von Mises stress by up to four times, depending on their length-to-thickness ratio. This effect becomes more pronounced with the existence of hydrogen in the pipeline network.

Keywords: pipeline network; hydrogen embrittlement; finite elements; structural integrity; crack

Academic Editor: Demos T. Tsahalis

Received: 30 April 2024
Revised: 16 January 2025
Accepted: 20 January 2025
Published: 24 January 2025

Citation: Vossou, C.; Koulocheris, D. Numerical Estimation of the Structural Integrity in an Existing Pipeline Network for the Transportation of Hydrogen Mixture in the Future. *Computation* **2025**, *13*, 26. https://doi.org/10.3390/computation13020026

1. Introduction

During the last decades, as the effects of global warming become more evident and the fossil fuels reserves are decreasing, the use of renewable and environmentally friendly energy carriers becomes imperative. Within this context, hydrogen is gaining growing attention as an alternative to fossil fuel. Its production methods are constantly explored, and research is conducted towards the production of green hydrogen. Research regarding the transport and distribution of hydrogen towards the end user is conducted, and it is raising practical questions such as whether the existing natural gas pipeline infrastructure can be utilized. In order to address this question, energetic and material restrictions should be recognized and encountered [1]. Studies concerning the use of natural gas pipeline infrastructure already exist in the literature [2,3].

One important restriction of the use of the natural gas pipeline infrastructure is the phenomenon of hydrogen embrittlement in metals. Hydrogen embrittlement (HE) is a complex, long-term process where hydrogen, due to its small atomic size, diffuses into the metal, reducing its ductility and increasing the likelihood of crack growth [4]. In the literature, five different failure mechanisms correlated to HE, namely, hydrogen-induced decohesion, hydrogen-enhanced local plasticity, hydrogen-induced phase transformation, hydrogen-enhanced strain-induced vacancy formation and adsorption-induced dislocation emission [4], are recognized. The extent of HE in a metal material is affected by the hydrogen concentration, the pressure and the temperature of the environment, the properties and the structure of the metal material and its stress state. The result of HE in a metal pipeline is influenced by the pipeline history and the pre-existence of cracks [2].

The effect of HE on metallic materials or metallic pipeline segments can be measured with complex experiments, or it can be computationally estimated. In experimental studies, it has been observed that HE affects the yield strength, the ultimate strength, the elongation to failure, the fatigue life and the hardening rate of the metallic materials [5–7]. As far as the computational estimation of the effect of HE is concerned, different methodologies can be used, ranging from nanoscale to macroscale modeling. For the macroscopic computational modeling of HE, the finite element (FE) method is commonly used. The macroscopic FE modeling of the HE can be performed either by simulating the fracture experiments conducted in metallic specimens that underwent HE [8–10] to quantitively estimate the change in their mechanical properties or by simulating segments of pipelines and incorporating HE as a change in the mechanical properties of the metallic materials [7,11–14] in order to predict their failure.

In this paper, six pipeline segments with different geometrical and mechanical characteristics have been simulated using FE analysis. The FE models were solved statically and transiently in order to investigate their structural integrity in terms of equivalent Von Mises stress. The effect of HE in these segments has been modeled as a decrease in the yield strength of the material, and the pipeline segments have been classified with regards to their safety factor. Then, a semi-elliptical crack has been modeled in the pipeline segments with the best and the worst structural integrity, and the effect of its orientation and length has been investigated.

2. Numerical Modeling of the Natural Gas Pipeline Segments

Within a natural gas pipeline network, pipeline segments with different geometrical and mechanical characteristics exist. In this paper, six different piping classes have been considered, all belonging in the same network for natural gas transportation. In Table 1, the nominal diameter and thickness of each piping class are presented. The thickness is defined as the half difference of the nominal outer minus the inner diameter of the pipeline segment.

Table 1. Nominal dimensions of each piping class.

Piping Class	Nominal Outer Diameter D (mm)	Nominal Thickness th (mm)
1C2	500	6.3
9C1	500	32
1G1	250	6.3
1S2	500	5.6
9S1	500	28
9C1U	500	20

As Table 1 depicts, two different nominal diameters are considered and five different nominal thicknesses. The mechanical properties of the linear elastic material used for each piping class, as they were retrieved from the literature, are outlined in Table 2.

Table 2. Mechanical properties of each piping class.

Piping Class	Material	Elastic Modulus (GPa)	Yield Tensile Strength (MPa)	Ultimate Tensile Strength (MPa)
1C2	P235GH	210 [15]	265	360
9C1	P265GH	217 [16]	265	410
1G1	P235GH GALV	210 [15]	265	360
1S2	1.4031/1.4307	190 [7]	195	500
9S1	1.4031/1.4307	190 [7]	195	500
9C1U	L360NB	205 [17]	360	460

Both the nominal dimensions and the mechanical properties of each piping class are in accordance with EN 13480—Metallic industrial piping design rules [18] and EN 1594—Gas infrastructure [19].

2.1. FE Models of the Intact Pipeline Segments

In order to perform a macroscopic FE analysis of a pipeline network without pre-existing damage full, three-dimensional FE models of pipeline segments belonging in each piping class have been built. The length of each segment was considered equal to 1000 mm in order to minimize the effect of the boundary conditions. Each segment has been considered straight. The geometrical models have been built in Solidworks® v.2024 3D CAD Software, while the FE models have been built in ANSYS® v. 2024R2 CAE Software. In Figure 1, the 3D CAD and the FE model of a segment belonging to piping class IC2 are presented.

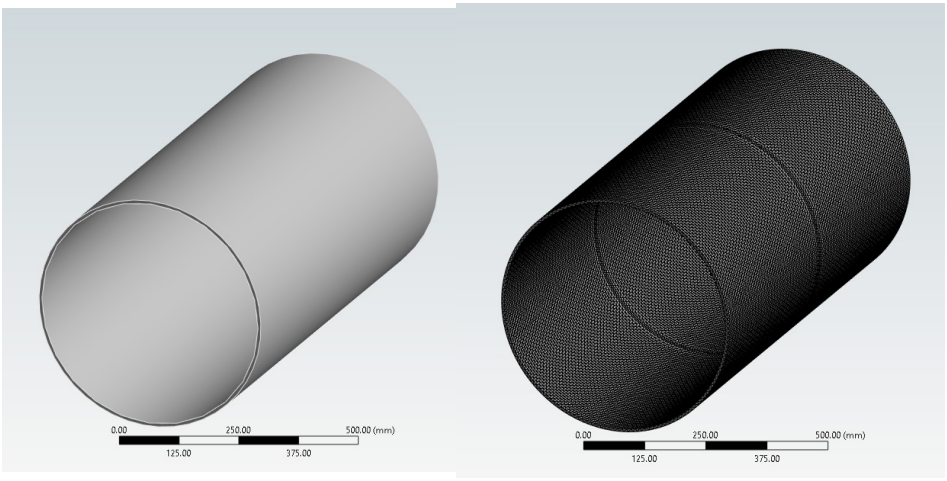

(**a**) (**b**)

Figure 1. Piping class 1C2 (**a**) 3D CAD model and (**b**) FE model.

For the meshing of all FE models, tetrahedral elements of type SOLID187 have been used. SOLID187 elements are defined by ten nodes, and they have three translational degrees of freedom (x, y, z) on each node [20]. The mesh was considered adaptive, and the element size was set at 5.0 mm after a convergence study with respect to the maximum

value of equivalent Von Mises stress. Table 3 displays the average element quality, the number of elements and the number of nodes of each FE model.

Table 3. Mesh properties of the FE models.

Piping Class	Average Element Quality	Number of Elements	Number of Nodes
1C2	0.82	106,756	214,390
9C1	0.85	411,277	618,132
1G1	0.82	52,701	105,831
1S2	0.78	106,759	214,384
9S1	0.84	376,004	571,847
9C1U	0.82	256,333	412,737

In order to estimate the structural integrity of each piping class during the typical operating conditions of the natural gas network, two types of analysis were performed for each piping class, one simulating the continuous fluid flow and one considering the closure or aperture of valves within the pipeline network. The first approach required a static analysis while the second one a transient analysis. In both approaches, a pressure load was applied on the inner surface of the pipeline segment with an outward direction, and the longitudinal degree of freedom of the nodes on the surfaces of the front and the rear edge of the pipeline was constrained.

For the static analysis, the pressure load was equal to 7.0 MPa, and it simulated the pressure exerted by the flowing fluid in the pipeline. The boundary conditions of the static analysis are demonstrated in Figure 2.

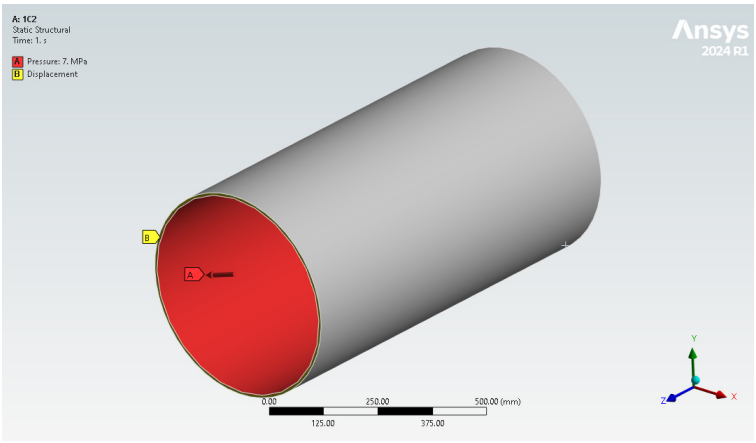

Figure 2. Boundary conditions of the static analysis.

For the transient analysis, the pressure load was applied in three loading steps. During the first loading step, the pressure had an initial value of 7.0 MPa, and within 0.2 s it reached, linearly, the maximum value P_{max}. During the second loading step, the pressure dropped back, linearly, to 7.0 MPa within 0.2 s. Finally, in the third load step, the value of the pressure load remained steady at 7.0 MPa for 0.6 s. This transient analysis simulates the rapid closure of the valve lasting 0.2 s, resulting in a water hammer phenomenon characterized by the transient increase and consequent decrease in pressure along the pipeline. In accordance with the literature, three values of P_{max}, equal to 7.3, 8.1 and 9.3 MPa, were used [7].

2.2. FE Models of the Pre-Cracked Pipeline Segments

In order to estimate the effect of a pre-existing crack in a pipeline segment of the natural gas infrastructure, FE models with a semi-elliptical crack have also been studied. In each FE model, a semi-elliptical crack was defined by its length (a), its depth (c) and its orientation. The length of the crack was correlated to the thickness of the pipeline segment (th) through the ratio $\frac{a}{th}$, and the depth of the crack was considered equal to $\frac{a}{2}$. In Table 4, the geometrical characteristics of the simulated cracks are listed for the piping class with the highest (9C1) and the lowest (1S2) nominal thickness.

Table 4. Different crack sizes.

$\frac{a}{th}$	Piping Class			
	9C1		1S2	
	a (mm)	c (mm)	a (mm)	c (mm)
0.1	3.20	1.60	0.56	0.28
0.2	6.40	3.20	1.12	0.56
0.3	9.60	4.80	1.68	0.84
0.4	12.80	6.40	2.24	1.12
0.5	16.00	8.00	2.80	1.40
0.6	19.20	9.60	3.36	1.68

In Figure 3a, the depth and the length of the crack are presented. Furthermore, in Figure 3, the area of the crack for the FE model of piping class 9C1 is illustrated for the crack with $\frac{a}{th} = 0.6$ in both the longitudinal (Figure 3b) and the transverse (Figure 3c) orientation. As it can be observed, the crack was modeled, with a fracture tool, in the middle of the length of the pipeline segment in order to avoid any influence of the boundary conditions in the results of the FE analysis.

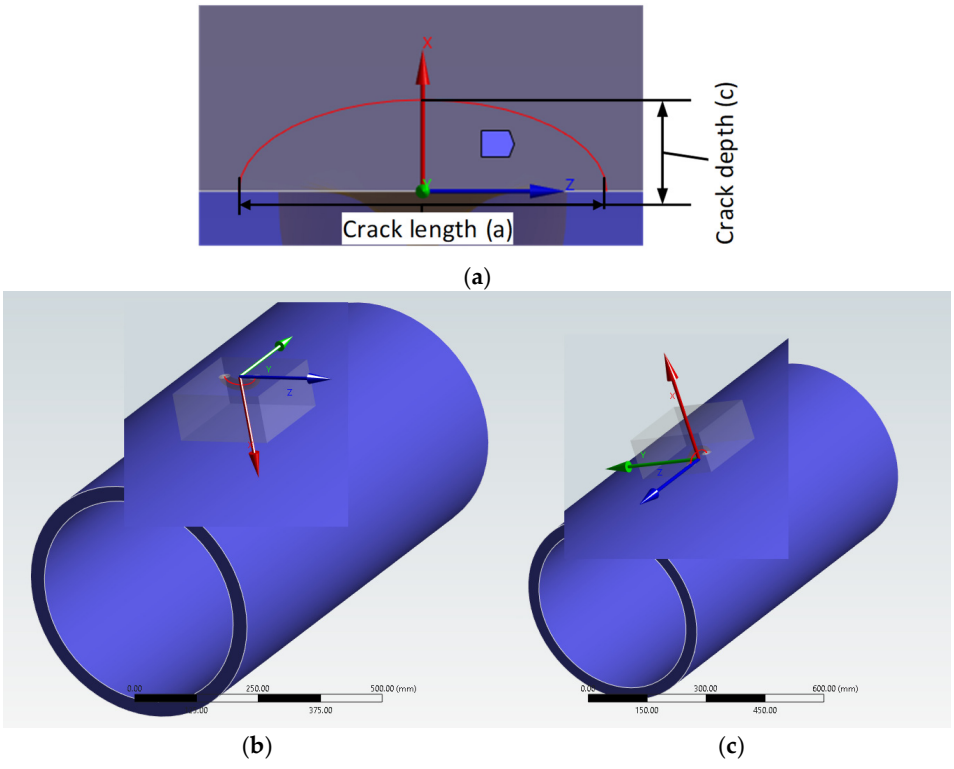

Figure 3. (**a**) Crack geometry, (**b**) longitudinal and (**c**) transverse crack area in piping class 9C1.

The element size of the vicinity of the crack has been reduced to 1.0 mm, after a convergence study, resulting in an increased number of FEs and nodes. In Figure 4, the mesh on the area of the crack is shown for both crack orientations for the piping class 1S2.

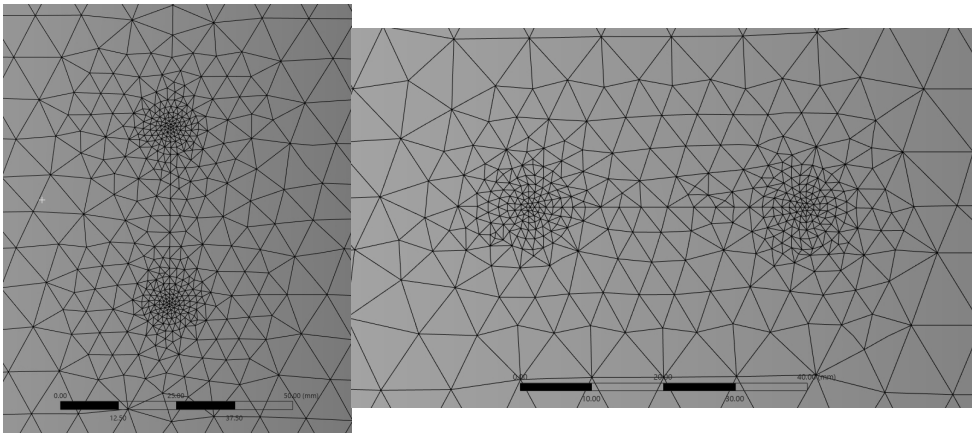

(**a**) (**b**)

Figure 4. Area of the (**a**) longitudinal and (**b**) transverse crack in piping class 1S2.

In Table 5, the mesh properties for all the FE models with the pre-existing crack are provided.

Table 5. Mesh properties of both models of pipeline segment with the semi-elliptical crack.

$\frac{a}{th}$	Piping Class					
	9C1			1S2		
	Average Element Quality	Number of Elements	Number of Nodes	Average Element Quality	Number of Elements	Number of Nodes
0.1	0.86	422,746	633,902	0.78	111,246	220,783
0.2	0.86	429,837	643,807	0.78	111,433	221,028
0.3	0.86	436,040	652,320	0.78	111,579	221,209
0.4	0.86	444,235	663,665	0.78	112,172	222,117
0.5	0.86	451,731	674,008	0.78	113,758	224,317
0.6	0.86	459,181	684,185	0.78	114,006	224,683

For each crack size and orientation, a static analysis with internal pressure equal to 7.0 MPa and a transient analysis with P_{max} equal to 9.3 MPa were performed, as described in Section 2.1.

3. Results

In this section, the results of the FE analysis of the intact and the pre-cracked pipeline segments are presented.

3.1. Intact Pipeline Network

In Table 6, the maximum value of equivalent Von Mises stress (SEQV) is presented for all the pipeline segments for the static analysis.

Table 6. Maximum SEQV value of the static analysis for all piping classes.

Piping Class	Maximum SEQV Value (MPa)
1C2	250
9C1	52
1G1	127
1S2	281
9S1	59
9C1U	88

The maximum value of SEQV is depicted in Table 7 for all pipeline segments and P_{max} for the transient analysis.

Table 7. Maximum SEQV value for the transient analysis for all piping classes.

Piping Class	P_{max} (MPa)		
	7.3	8.1	9.3
	Maximum SEQV Value (MPa)		
1C2	261	288	332
9C1	54	60	69
1G1	131	146	168
1S2	293	325	373
9S1	61	78	68
9C1U	92	102	117

3.2. Pipeline Network with Pre-Existing Crack

For the evaluation of the structural integrity of the pipeline segments with the pre-existing crack, both the maximum SEQV value and the stress intensity factor (SIF) of the crack are investigated. In ANSYS v. 2024R2 software, three SIFs are calculated, correlated to different modes of fracture associated with the direction of the developed forces and moments on the tip of the crack. Each SIF corresponds to a fracture mode as follows. SIF1 is associated with an opening mode where the force is perpendicular to the crack faces, SIF2 is a sliding mode (crack faces slide) where the forces are parallel to the crack faces, and SIF3 is correlated to a shearing mode associated with torsional moments [21]. SIF is correlated to the energy release rate G through Equation (1):

$$SIF^2 = E' \cdot G \quad (1)$$

The energy release rate is calculated through Equation (2):

$$G = \frac{\pi \cdot \sigma^2 \cdot \alpha}{E} \quad (2)$$

where α is the crack length, σ is the applied stress, E is the modulus of elasticity, and E' depends on whether the problem is plain stress or plain strain.

The results are presented for both longitudinal and transverse pre-existing cracks.

3.2.1. Longitudinal Crack

The maximum SEQV value is presented in Table 8 for all ratios $\frac{a}{th}$ of the longitudinal crack, for both the static and the transient analysis.

Table 8. Maximum value of SEQV for the longitudinal crack.

$\frac{a}{th}$	Piping Class			
	9C1		1S2	
	Static	Transient	Static	Transient
	Maximum SEQV Value (MPa)			
0.1	96	127	337	448
0.2	134	178	388	516
0.3	143	189	435	578
0.4	176	234	510	677
0.5	196	260	556	738
0.6	218	289	636	845

In Figure 5, the SEQV contour in the vicinity of the longitudinal crack with $\frac{a}{th}$ ratio equal to 0.6 is presented for the static analysis.

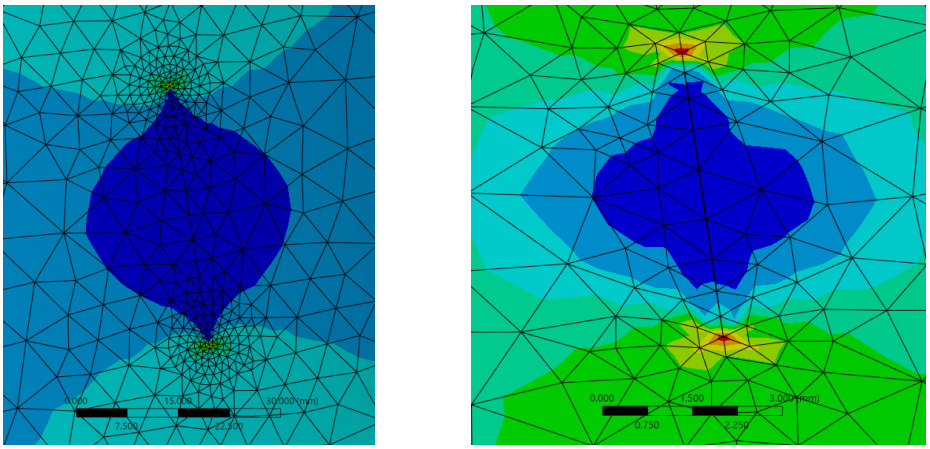

(**a**) (**b**)

Figure 5. SEQV contour for the longitudinal crack area in piping class (**a**) 9C1 and (**b**) 1S2.

In Table 9, the SIF values for the static analysis are presented for both pipeline segments and all $\frac{a}{th}$ ratios.

Table 9. SIF values of the longitudinal crack in static analysis.

$\frac{a}{th}$	Piping Class					
	9C1			1S2		
	SIF1	SIF2	SIF3	SIF1	SIF2	SIF3
	MPa·$\sqrt{m}$					
0.1	99.85	0.10	1.69	209.38	7.05	9.32
0.2	141.50	0.19	1.46	245.72	9.27	11.43
0.3	173.11	0.22	1.15	422.28	1.14	−0.18
0.4	199.94	0.25	0.57	476.53	9.83	0.12
0.5	224.97	0.35	0.77	573.17	11.26	2.14
0.6	248.14	0.41	0.77	641.33	0.85	11.24

Finally, in Table 10, the values of the SIF on the end of the first loading step for the transient analysis are depicted for both pipeline segments and all $\frac{a}{th}$ ratios.

Table 10. SIF for the transient analysis of the pipeline segment with a longitudinal crack.

$\frac{a}{th}$	Piping Class					
	9C1			1S2		
	SIF1	SIF2	SIF3	SIF1	SIF2	SIF3
	MPa·$\sqrt{m}$					
0.1	106.41	0.11	1.81	223.14	7.51	9.93
0.2	150.79	0.20	1.56	261.87	9.87	12.19
0.3	184.48	0.23	1.23	450.03	1.22	−0.19
0.4	213.08	0.27	0.60	507.84	10.48	0.12
0.5	239.75	0.38	0.82	610.84	12.00	2.28
0.6	264.44	0.43	0.82	683.47	0.91	11.97

The values of the SIF provided in Tables 9 and 10 correspond to the maximum values obtained on the highest point of the crack.

3.2.2. Transverse Crack

The maximum value of SEQV, for both the static and the transient analysis of pipeline segments belonging in piping classes 9C1 and 1S2 with a transverse crack, is presented in Table 11. Each line of Table 11 corresponds to a different $\frac{a}{th}$ ratio.

Table 11. Maximum value of SEQV for the transverse crack.

$\frac{a}{th}$	Piping Class			
	9C1		1S2	
	Static	Transient	Static	Transient
	Maximum SEQV Value (MPa)			
0.1	51.39	68.27	309.09	410.63
0.2	51.40	68.28	302.19	401.47
0.3	51.42	68.32	300.83	399.66
0.4	54.81	72.81	306.98	407.83
0.5	57.76	76.73	304.06	403.95
0.6	61.46	81.65	317.38	421.64

In Figure 6, the SEQV contours on the area of the transverse crack are presented for the static analysis of both piping classes for $\frac{a}{th}$ equal to 0.6.

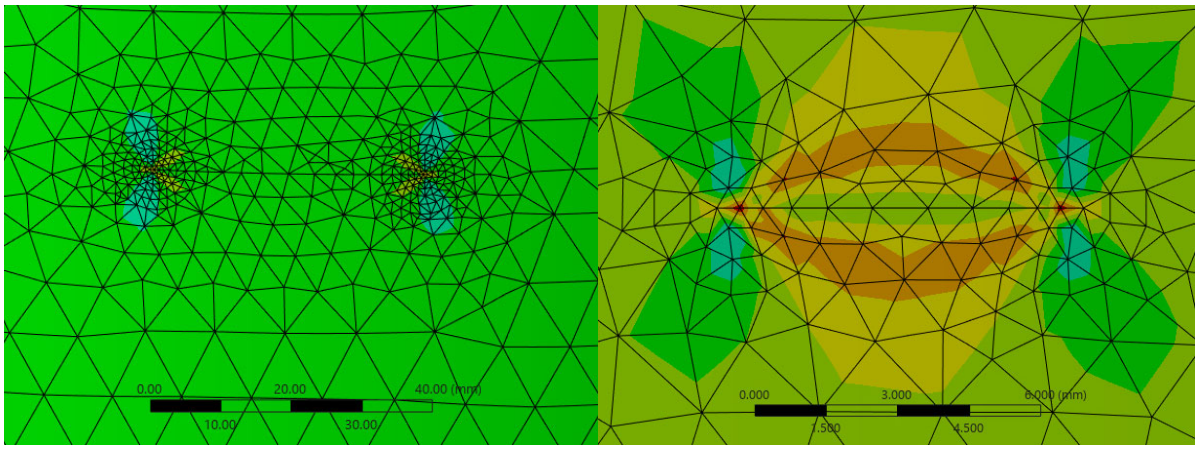

(**a**) (**b**)

Figure 6. SEQV contour for the transverse crack area in piping class (**a**) 9C1 and (**b**) 1S2.

In Table 12, the values of SIF for the static analysis are presented for both pipeline segments and all $\frac{a}{th}$ ratios.

Table 12. SIF value of the transverse crack in static analysis.

$\frac{a}{th}$	Piping Class					
	9C1			1S2		
	SIF1	SIF2	SIF3	SIF1	SIF2	SIF3
	MPa·$\sqrt{m}$					
0.1	26.10	0.19	0.62	62.17	−5.17	2.08
0.2	37.35	0.05	0.50	70.89	−1.03	3.35
0.3	46.09	0.07	0.64	122.79	0.21	1.00
0.4	53.66	0.08	0.42	148.00	3.04	3.78
0.5	60.77	0.11	0.15	169.86	0.19	3.04
0.6	67.60	0.08	0.17	189.09	1.41	0.58

Finally, Table 13 depicts the SIF values at the end of the first loading step for the transient analysis, for both pipeline segments and all $\frac{a}{th}$ ratios.

Table 13. SIF value of the transverse crack in transient analysis.

$\frac{a}{th}$	Piping Class					
	9C1			1S2		
	SIF1	SIF2	SIF3	SIF1	SIF2	SIF3
	MPa·$\sqrt{m}$					
0.1	27.82	0.21	0.66	66.25	−5.51	2.22
0.2	39.80	0.05	0.53	75.55	−1.09	3.57
0.3	49.12	0.08	0.68	130.86	0.22	1.07
0.4	57.19	0.09	0.45	157.72	3.24	4.03
0.5	64.76	0.12	0.16	181.02	0.21	3.24
0.6	72.04	0.09	0.19	201.51	1.50	0.62

4. Discussion

In total, 24 FE models of intact pipeline segments belonging to six piping classes have been created. Each model was simulated in four different loading conditions. Furthermore, 12 FE models of pipeline segments with pre-existing cracks of different orientation and size have been created and solved in two different loading conditions each.

As it is observed in Table 14, for each piping class, a ratio of nominal thickness (th) to nominal diameter (D) can be calculated.

Table 14. The $\frac{th}{D}$ ratio for each piping class.

Piping Class	$\frac{th}{D}$
1C2	0.013
9C1	0.064
1G1	0.025
1S2	0.011
9S1	0.056
9C1U	0.040

Piping class 1S2 exhibits the lowest value of $\frac{th}{D}$, while piping class 9C1 exhibits the highest one.

4.1. Intact Pipeline Network

The mesh quality of the FE models, presented in Table 3, ranges from 0.78 to 0.85, depending on the thickness of the pipeline segment. The results of the static analysis indicate that the highest value of SEQV appeared for piping class 1S2, and it was equal to 281 MPa, while the lowest value appeared for piping class 9C1, and it was equal to 52 MPa.

In Figure 7, the $\frac{th}{D}$ for each class is correlated to the highest value of SEQV, for the static analyses. As it can be observed, the correlation between $\frac{th}{D}$ and the maximum value of SEQV is non-linear.

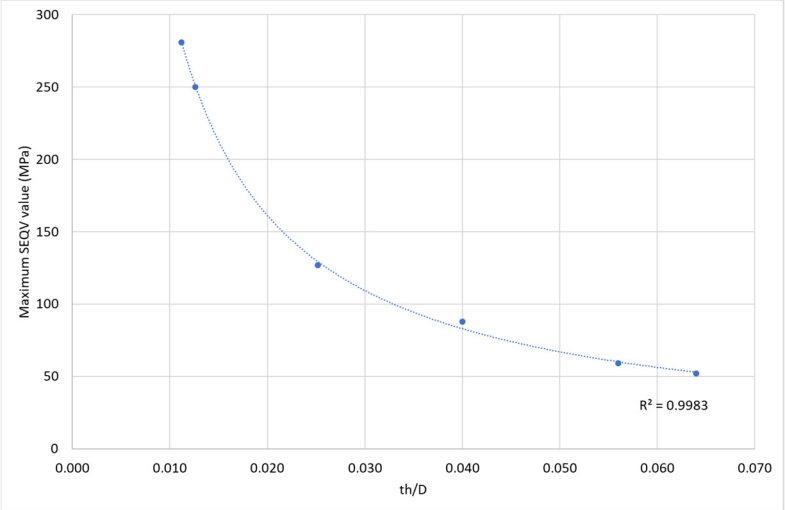

Figure 7. Maximum SEQV value for $\frac{th}{D}$ correlation for the static analysis.

In Figure 8, the safety factor of each piping class is illustrated with respect to its yield strength.

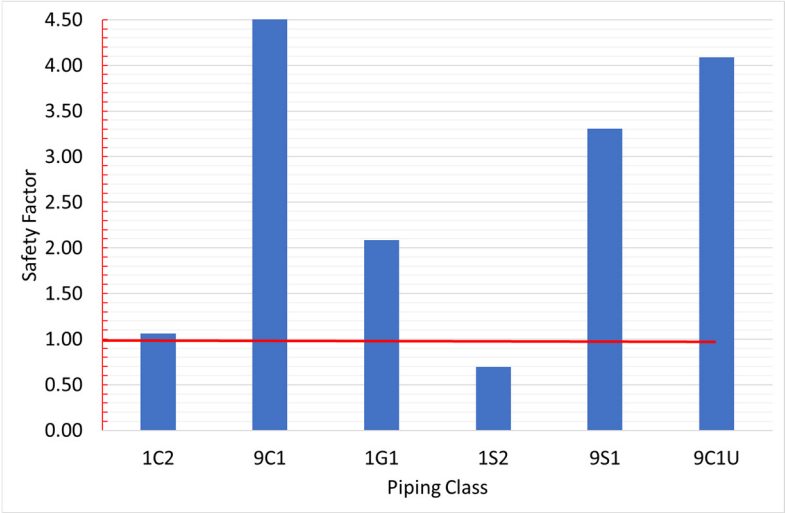

Figure 8. Safety factor for all piping classes for the static analysis.

As far as the transient analysis is concerned, in Table 7 it is shown that the worst-case scenario is the rapid closure of the valve with P_{max} equal to 9.3 MPa since it results in the highest values of SEQV.

In Figure 9, the value of $\frac{th}{D}$ of each piping class is correlated to the highest value of SEQV computed in the transient analyses. As it can be observed, the correlation between $\frac{th}{D}$ and the maximum value of SEQV is non-linear.

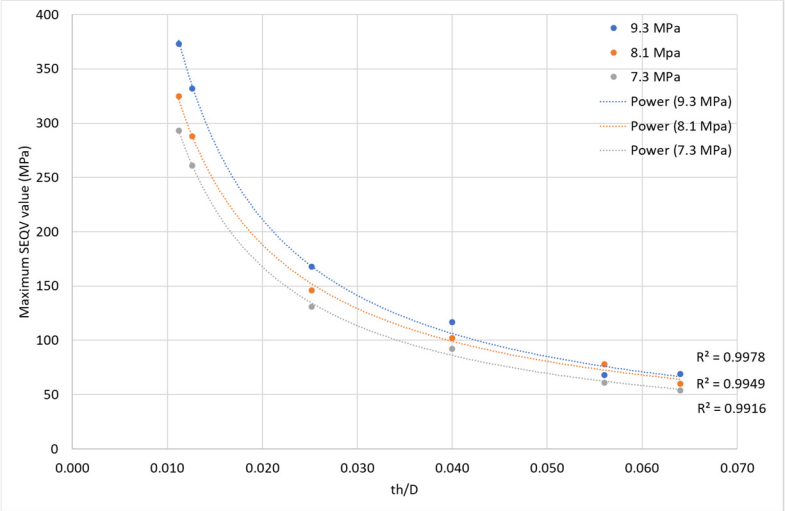

Figure 9. Maximum SEQV value to $\frac{th}{D}$ ratio correlation for the transient analysis.

In Figure 10, the safety factor is illustrated for all piping classes in the worst-case scenario of the transient analysis.

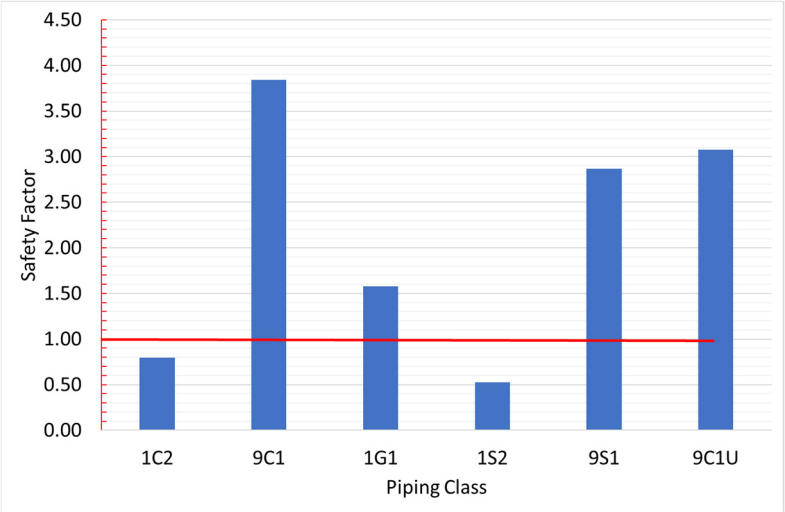

Figure 10. Safety factor for all piping classes for the transient analysis with P_{max} = 9.3 MPa.

In both Figures 8 and 10, the red line illustrates the limit value of the safety factor of unity, which signifies yield initiation of the pipeline material. Figure 7 indicates that piping classes 1S2 should not be used in parts of the network where the pressure is 7 MPa or higher. On the other hand, Figure 9 shows that piping classes 9C1, 1G1, 9S1 and 9C1U can successfully withstand internal pressure higher than 9.3 MPa without yielding.

In Figure 11, the safety factor with respect to the ultimate strength of each piping class is presented for both the static and the transient analysis with P_{max} equal to 9.3 MPa. The red line in Figure 11 illustrates the limit value of the safety factor of unity, which signifies break initiation of the pipeline material.

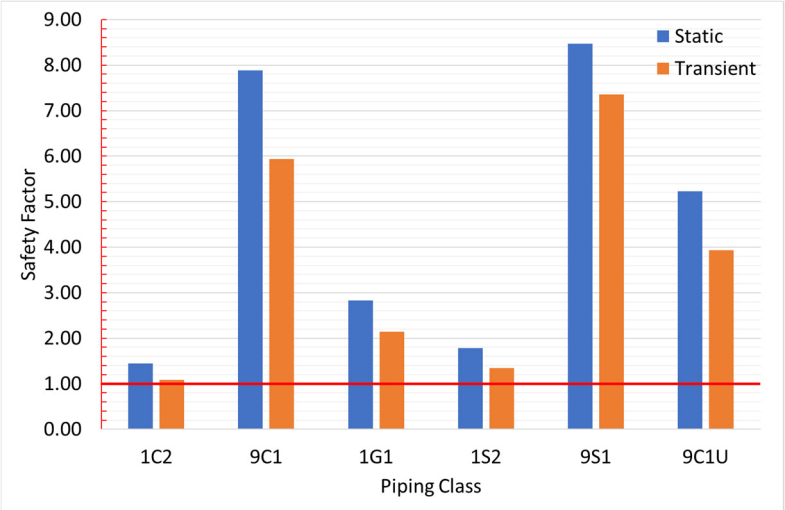

Figure 11. Safety factor for all piping classes for both the static and the transient analysis with respect to ultimate strength.

Figure 11 indicates that no piping class is susceptible to fracture, since the maximum value of SEQV in all FE models is less than the corresponding ultimate strength.

4.2. Pipeline Network with Pre-Existing Crack

In order to evaluate the influence of a pre-existing crack in a pipeline segment, static and transient analyses with P_{max} equal to 9.3 MPa were performed for piping classes 9C1 and 1S2 exhibiting the highest and the lowest value of $\frac{th}{D}$, respectively. The simulation of a semi-elliptical crack increases the number of the FEs and the nodes without altering the mesh quality, as Table 5 makes obvious. In Tables 8 and 11, it is shown that regardless of the orientation of the crack, the maximum value of SEQV in both the static and the transient analysis increases with the increase in the length of the crack. In Figure 12, the ratio of the maximum SEQV value of the pre-cracked pipeline segment to the maximum SEQV value of the intact pipeline segment with respect to $\frac{a}{th}$ ratio is presented for piping class 9C1.

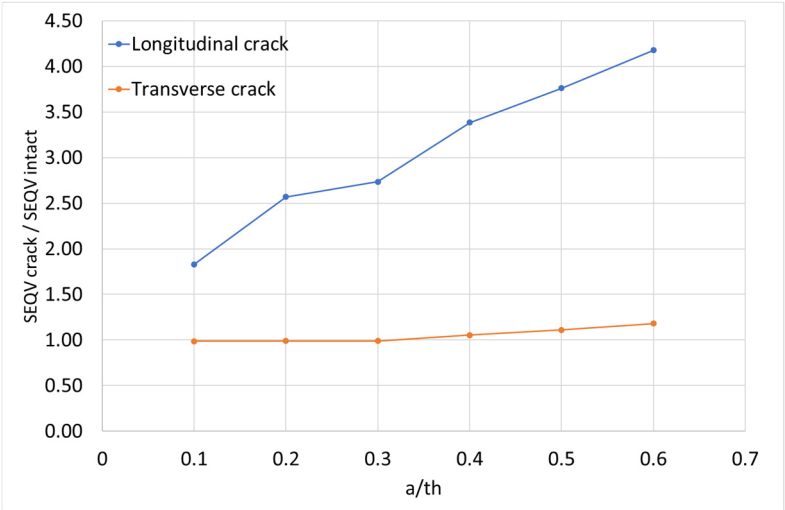

Figure 12. Increase in the maximum SEQV value due to the existence of a crack in piping class 9C1.

The same quantities are presented for piping class 1S2 for both the longitudinal and the transverse crack in Figure 13. For this piping class, the effect of the longitudinal crack is less pronounced.

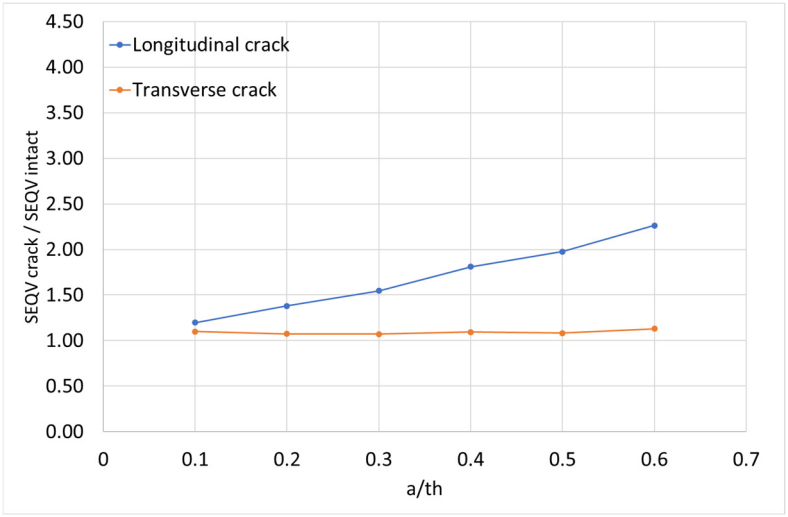

Figure 13. Increase in the maximum SEQV value due to the existence of a crack in piping class 1S2.

In both Figures 12 and 13, it is evident that the existence of a longitudinal crack increases the maximum value of SEQV. Furthermore, as the value of $\frac{a}{th}$ of the crack increases, the influence of the crack is more severe. For piping class 9C1, a longitudinal crack with $\frac{a}{th}$ equal to 0.6 increases the maximum value of SEQV four times with respect to that of the intact pipeline segment.

The same increase in the maximum SEQV value with the presence of a longitudinal crack can be observed in Table 8 for the transient analysis.

The dominance of fracture mode I is indicated in Tables 9 and 12 since SIF1 has the highest value in all simulations. The value of SIF1 increases with the increase in $\frac{a}{th}$. In Figure 14, the SIF1 values are presented for the static analysis of both piping classes.

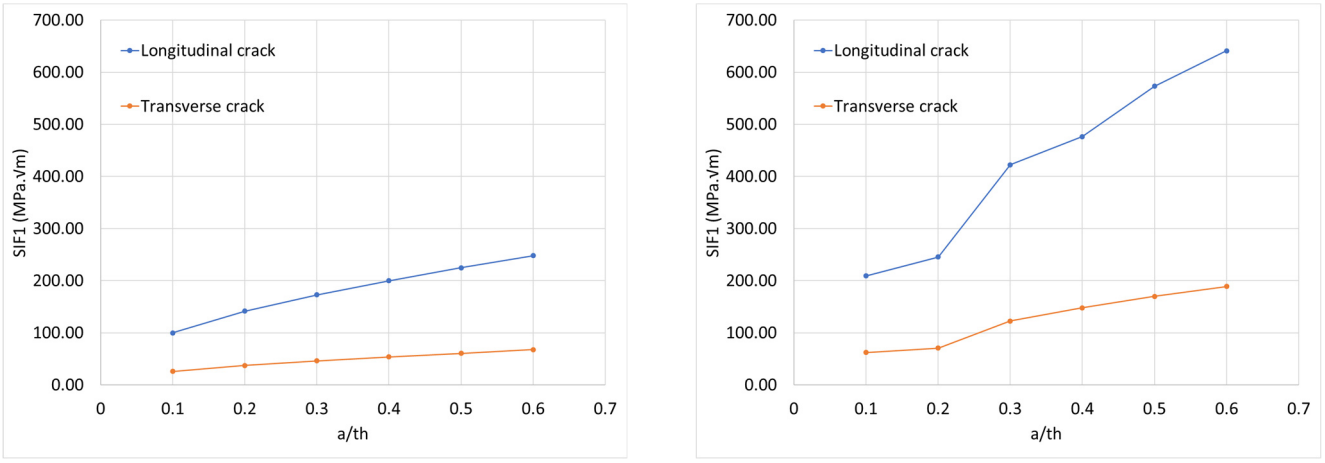

Figure 14. SIF1 of the longitudinal and the transverse crack in static analysis for piping class (**a**) 9C1 and (**b**) 1S2.

According to the literature [7], the ratio of the SIF1 to the fracture toughness of the material defines the non-dimensional crack driving force. The fracture toughness (K_{IC}) of the API 5L X52 steel, which is a typical steel used for natural gas pipeline networks, has been found equal to 95.6 MPa$\cdot\sqrt{m}$. A non-dimensional crack driving force can be calculated as $\frac{K_{IC}}{SIF1}$. In Figure 15, this non-dimensional crack driving force is illustrated for all FE models with pre-existing damage, indicating that for both the longitudinal and the transverse crack, the non-dimensional driving force increases as ratio $\frac{a}{th}$ increases.

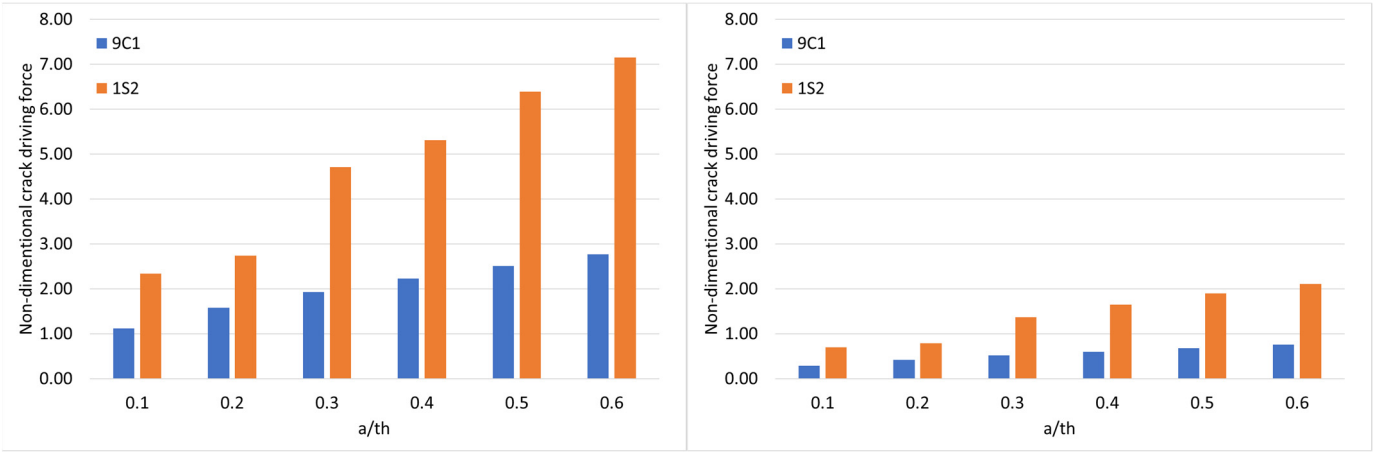

Figure 15. Non-dimensional crack driving force for the (**a**) longitudinal and (**b**) transverse crack area in static analysis for piping classes 9C1 and 1S2.

In Figure 16, the value of SIF1 along the length of the crack is provided for the crack with the maximum $\frac{a}{th}$ for both orientations, all analysis and both piping classes.

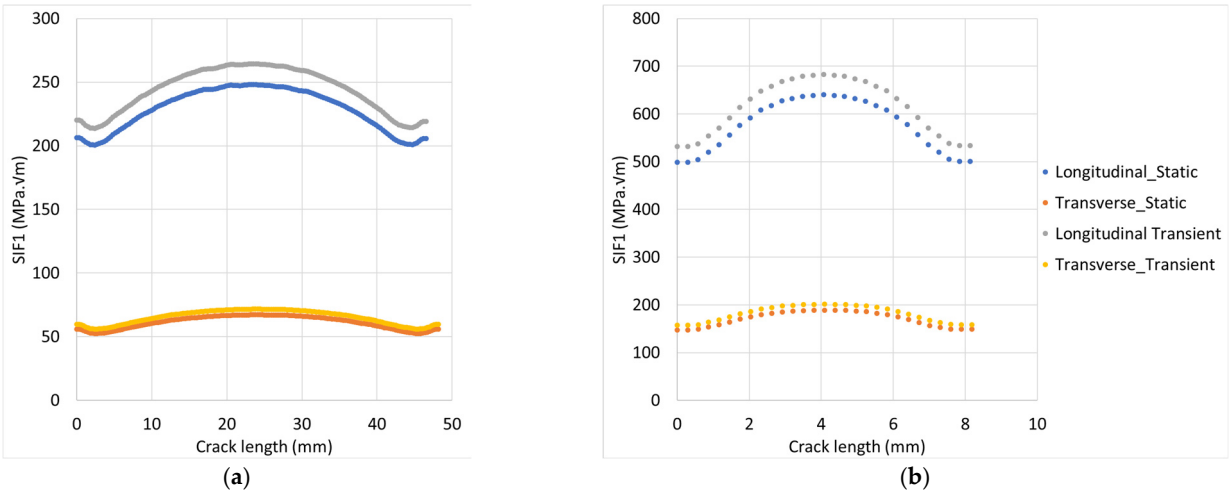

Figure 16. SIF1 along the crack length for piping class (**a**) 9C1 and (**b**) 1S2.

In all cases, the highest value of SIF1 is observed in the middle of the crack length.

4.3. Hydrogen Embrittlement

As it has already been mentioned, hydrogen, due to its small atomic size, has the tendency to infiltrate metallic materials and consequently reduce their ductility [22,23].

According to the literature, the macroscopic effect of hydrogen in different metallic materials used in pipeline networks can cause a decrease in yield and ultimate strength, elongation to fracture or fracture toughness. In Table 15, some of the experimental results supporting this clause are summarized [7].

Table 15. Effect of hydrogen embrittlement on the mechanical properties of metals.

Material	Changes in	
	Yield Tensile Strength (%)	Ultimate Tensile Strength (%)
API 5L X52	2.5	
API 5L X70	8.0	12.7
API Grade 60	2.0	7.0

As observed, in Table 15, the decrease in yield strength ranges from 2 to 8%, while in ultimate strength from 7 to 13%, depending on the material itself. The influence of hydrogen embrittlement is more severe in the ultimate strength of the material. Incorporating the results concerning the tensile strength presented in Figures 8 and 10 and assuming a decrease of 10% in yield strength of each material, the safety factor has been recalculated and presented in Figure 17. It is obvious that in both analyses, static and transient, the pipeline segments belonging in piping classes 1C2 and 1S2 yield regardless of the approach.

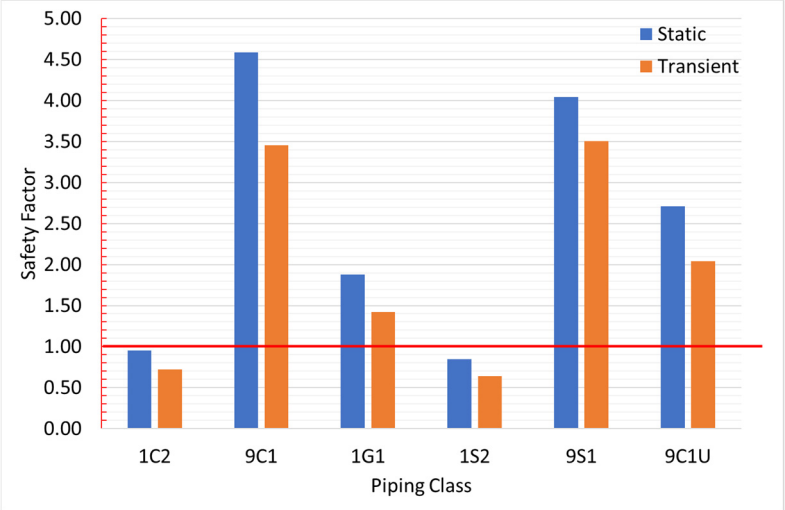

Figure 17. Safety factor for all piping classes for both the static and the transient analysis considering mechanical properties deterioration due to hydrogen embrittlement.

Boukortt et al. [13] report experiments that indicate that the fracture toughness of metallic materials also decreases due to the presence of hydrogen. In more details, a decrease of 14% in the value of the fracture toughness in API 5L X52, 5% in API 5L X70 and 1% in API 5L X100 have been recorded. Furthermore, in the literature [24], it is mentioned that when steel is exposed to hydrogen gas under pressure up to 6.9 MPa, the fracture toughness can decrease by as much as 50% but still remain over 70 MPa$\cdot\sqrt{\text{m}}$.

Due to lack of information for the specific alloys used in the piping classes within this study, and keeping this overall minimum, Figure 18 presents the ratio of the stress intensity factor to the fracture toughness.

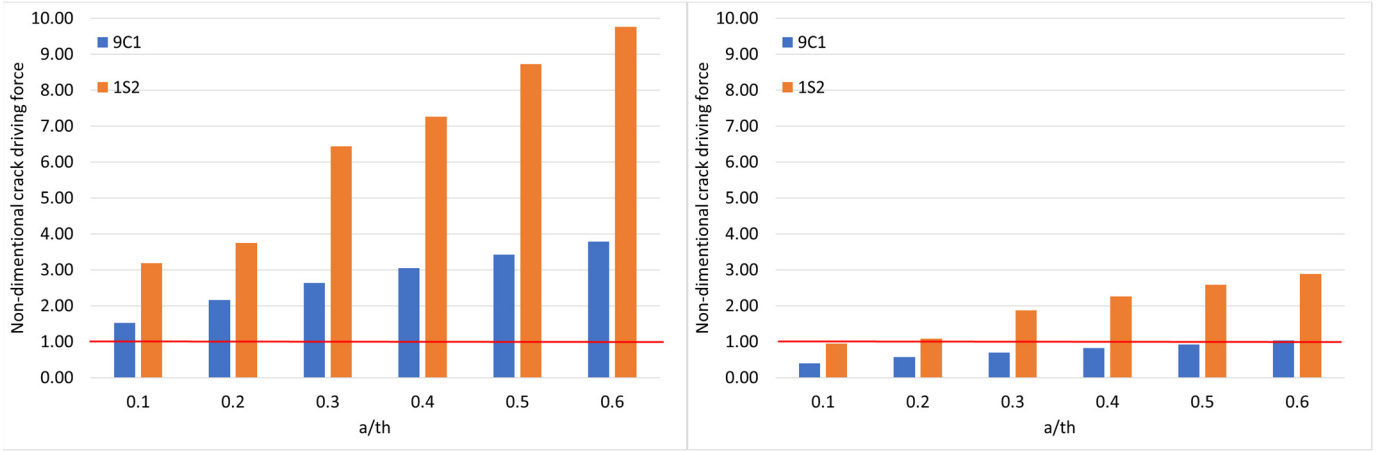

Figure 18. Non-dimensional crack driving force for the (**a**) longitudinal and (**b**) transverse crack area in static analysis for piping classes 9C1 and 1S2 considering hydrogen embrittlement.

Figure 18 depicts the fact that all the longitudinal cracks, regardless of the $\frac{a}{th}$ value, compromise the structural integrity of the pipeline segment. As far as the transverse cracks are concerned, their effect is crucial to the transient analysis and only when $\frac{a}{th}$ is equal to 0.3 or greater.

5. Conclusions

In this paper, the structural integrity of pipeline segments attributed to six different piping classes, belonging to an already existing pipeline network for the transportation of natural gas, has been investigated, macroscopically, using the FE method. The use of these pipeline segments for the transportation of pure hydrogen or a mixture of hydrogen and natural gas has been investigated by macroscopically modeling the phenomenon of HE. HE makes metallic materials more susceptible to fracture. As the concentration of hydrogen in the mixture rises, so will it rise the effect of the hydrogen on the metallic material of the pipeline network. On a macroscopic level, the effect of HE causes a decrease in the yield strength, the ultimate strength and the fracture toughness of the material itself. In order to simulate the influence of HE, experimental data available in the literature have been used.

Each piping class corresponds to a different $\frac{th}{D}$ ratio and metallic material. Each pipeline segment has been subjected to four different loading cases, one static and three transient, in order to retrieve the maximum value of SEQV. Taking under consideration the different yield and ultimate strength of metallic material, the more susceptible piping class is 1S2, which has yield strength equal to 265 MPa. More specifically, during the transient analysis with P_{max} equal to 9.3 MPa, the ratio of yield strength to the maximum value of SEQV is equal to 0.5. On the other hand, no piping class under any loading condition is susceptible to fracture under normal operating conditions. The lower ratio of the maximum value of the ultimate strength to the maximum value of SEQV is equal to 1.1, and it is met in piping class 1C2, which has an ultimate strength equal to 360 MPa.

Moreover, the effect of a semi-elliptical crack in the structural integrity of the pipeline segments belonging to piping classes 9C1 and 1S2 has been explored in loading cases simulating normal flow with pressure equal to 7.0 MPa and rapid valve closure with P_{max} equal to 9.3 MPa. The effect of the orientation of the crack has been analyzed, along with the effect of the size of the crack. The results indicated that the maximum value of SEQV increases with the length of the crack for both piping classes, regardless of the orientation of the crack and the loading condition. The same trend is also observed for the SIF values. The SIF with the highest value is SIF1, which is correlated to failure mode I, where the opening force is perpendicular to the crack faces. As far as the orientation of the crack is concerned, the longitudinal cracks undermine more the structural integrity of the pipeline segment compared to transverse ones. The presence of a longitudinal crack can result in an increase in the maximum value of SEQV by four times, while the transverse crack resulted in an increase of the maximum value of SEQV by less than 20%. When the maximum value of SIF is compared to the fracture toughness, it is shown that the structural integrity of the pipeline segment belonging to both piping classes is compromised with the existence of a longitudinal crack, regardless of the value of $\frac{a}{th}$. Nevertheless, piping class 9C1 can sustain a transverse crack with $\frac{a}{th}$ up to 0.6, while piping class 1S2 can sustain a transverse crack with $\frac{a}{th}$ up to 0.2.

When HE occurs, both piping classes 1C2 and 1S2 are susceptible to fracture. Furthermore, the results indicated that the structural integrity of piping class 9C1 is compromised with a transverse crack with $\frac{a}{th}$ higher than 0.5, while the structural integrity of piping class 1S2 is compromised with a transverse crack with $\frac{a}{th}$ higher than 0.1.

The computational model presented in this study is extensive, fully parametric and incorporates real-world geometrical data of the piping classes. This computational model

can be extended, in the future, in order to computationally investigate the fatigue behavior of intact and pre-cracked pipeline segments under hydrogen embrittlement. This FE model could provide insights to assist the ongoing research on the very high-cycle fatigue behavior of metals in a hydrogen environment [25]. Future research could also focus on HE experiments targeted to specific piping classes. These experimental results could enhance the macroscopic modeling of HE, making the proposed computational model a robust tool for the preliminary analysis of the structural integrity of a pipeline network constructed for the transport of natural gas and, eventually, used for the transport of a hydrogen–natural gas mixture.

Author Contributions: Conceptualization, D.K. and C.V.; methodology, D.K. and C.V.; software, C.V.; validation, D.K. and C.V.; formal analysis, D.K. and C.V.; investigation, D.K. and C.V.; data curation, D.K. and C.V.; writing—original draft preparation, C.V.; writing—review and editing, D.K.; visualization, C.V.; supervision, D.K. All authors have read and agreed to the published version of the manuscript.

Funding: This research received no external funding.

Data Availability Statement: Data are contained within the article.

Conflicts of Interest: The authors declare no conflicts of interest.

References

1. Haeseldonckx, D.; D'haeseleer, W. The use of the natural-gas pipeline infrastructure for hydrogen transport in a changing market structure. *Int. J. Hydrogen Energy* **2007**, *32*, 1381–1386. [CrossRef]
2. Messaoudani, Z.L.; Rigas, F.; Hamid, M.D.B.; Hassan, C.R.C. Hazards, safety and knowledge gaps on hydrogen transmission via natural gas grid: A critical review. *Int. J. Hydrogen Energy* **2016**, *41*, 17511–17525. [CrossRef]
3. Jia, G.; Lei, M.; Li, M.; Xu, W.; Li, R.; Lu, Y.; Cai, M. Hydrogen embrittlement in hydrogen-blended natural gas transportation systems: A review. *Int. J. Hydrogen Energy* **2023**, *48*, 32137–32157. [CrossRef]
4. Barrera, O.; Bombac, D.; Chen, Y.; Daff, T.D.; Galindo-Nava, E.; Gong, P.; Haley, D.; Horton, R.; Katzarov, I.; Kermode, J.R.; et al. Understanding and mitigating hydrogen embrittlement of steels: A review of experimental, modelling and design progress from atomistic to continuum. *J. Mater. Sci.* **2018**, *53*, 6251–6290. [CrossRef]
5. Djukic, M.B.; Bakic, G.M.; Zeravcic, V.S.; Sedmak, A.; Rajicic, B. Hydrogen embrittlement of industrial components: Prediction, prevention, and models. *Corrosion* **2016**, *72*, 943–961. [CrossRef] [PubMed]
6. Wasim, M.; Djukic, M.B. Hydrogen embrittlement of low carbon structural steel at macro-, micro-and nano-levels. *Int. J. Hydrogen Energy* **2020**, *45*, 2145–2156. [CrossRef]
7. Bouledroua, O.; Hafsi, Z.; Djukic, M.B.; Elaoud, S. The synergistic effects of hydrogen embrittlement and transient gas flow conditions on integrity assessment of a precracked steel pipeline. *Int. J. Hydrogen Energy* **2020**, *45*, 18010–18020. [CrossRef]
8. Chatzidouros, E.V.; Papazoglou, V.J.; Tsiourva, T.E.; Pantelis, D.I. Hydrogen effect on fracture toughness of pipeline steel welds, with in situ hydrogen charging. *Int. J. Hydrogen Energy* **2011**, *36*, 12626–12643. [CrossRef]
9. Chatzidouros, E.V.; Traidia, A.; Devarapalli, R.S.; Pantelis, D.I.; Steriotis, T.A.; Jouiad, M. Effect of hydrogen on fracture toughness properties of a pipeline steel under simulated sour service conditions. *Int. J. Hydrogen Energy* **2018**, *43*, 5747–5759. [CrossRef]
10. Wang, M.Q.; Akiyama, E.; Tsuzaki, K. Fracture criterion for hydrogen embrittlement of high strength steel. *Mater. Sci. Technol.* **2006**, *22*, 167–172. [CrossRef]
11. Vasco, M.C.; Tserpes, K.; Pantelakis, S.G. Numerical simulation of tensile behavior of corroded Aluminum alloy 2024 T3 considering the hydrogen embrittlement. *Metals* **2018**, *8*, 56. [CrossRef]
12. Zhou, R.; Gu, X.; Bi, S.; Wang, J. Finite element analysis of the failure of high-strength steel pipelines containing group corrosion defects. *Eng. Fail. Anal.* **2022**, *136*, 106203. [CrossRef]
13. Boukortt, H.; Amara, M.; Meliani, M.H.; Bouledroua, O.; Muthanna, B.G.N.; Suleiman, R.K.; Pluvinage, G. Hydrogen embrittlement effect on the structural integrity of API 5L X52 steel pipeline. *Int. J. Hydrogen Energy* **2018**, *43*, 19615–19624. [CrossRef]
14. Shuai, Y.; Zhang, X.; Huang, H.; Feng, C.; Cheng, Y.F. Development of an empirical model to predict the burst pressure of corroded elbows of pipelines by finite element modelling. *Int. J. Press. Vessel. Pip.* **2022**, *195*, 104602. [CrossRef]
15. Konjatic, P.; Konjatic, A.; Slisuric, R. Stress and Strain Analysis of Connection of Pipes with Flat Ends. *Innovations* **2018**, *6*, 102–105.
16. Singh, D.K.; Villamayor, A.; Hazra, A. Numerical and experimental analysis of loctite adhesive composite wrapping on EN 10028 steel pipe. *Mater. Today Proc.* **2021**, *44*, 4158–4165. [CrossRef]

17. Lukács, J.; Nagy, G.; Török, I.; Égert, J.; Pere, B. Experimental and numerical investigations of external reinforced damaged pipelines. *Procedia Eng.* **2010**, *2*, 1191–1200. [CrossRef]
18. *EN 13480*; Metallic Industrial Piping. European Committee for Standardization: Brussels, Belgium, 2017.
19. *EN 1594*; Gas Infrastructure—Pipelines for Maximum Operating Pressure over 16 Bar-Functional Requirements. European Committee for Standardization: Brussels, Belgium, 2024.
20. Ansys Inc. *Ansys Element—Release 2024R1*; Ansys Inc.: Canonsburg, PA, USA, 2024.
21. Nor, K.M.; Ibrahim, M.N.; Choiron, M.A. An overview of fracture mechanics with ANSYS. *Mech. Eng.* **2018**, *10*, 59–67.
22. Dwivedi, S.K.; Vishwakarma, M. Hydrogen embrittlement in different materials: A review. *Int. J. Hydrogen Energy* **2018**, *43*, 21603–21616. [CrossRef]
23. Sobola, D.; Dallaev, R. Exploring Hydrogen Embrittlement: Mechanisms, Consequences, and Advances in Metal Science. *Energies* **2024**, *17*, 2972. [CrossRef]
24. Dadfarnia, M.; Sofronis, P.; Brouwer, J.; Sosa, S. Assessment of resistance to fatigue crack growth of natural gas line pipe steels carrying gas mixed with hydrogen. *Int. J. Hydrogen Energy* **2019**, *44*, 10808–10822. [CrossRef]
25. Yang, S.; De Jesus, A.M.; Meng, D.; Nie, P.; Darabi, R.; Azinpour, E.; Zhu, S.-P.; Wang, Q. Very high-cycle fatigue behavior of steel in hydrogen environment: State of the art review and challenges. *Eng. Fail. Anal.* **2024**, *166*, 108898. [CrossRef]